Redetection of the ionospheric signature of Saturn's "Ring Rain"

O'Donoghue, J. ORCID: https://orcid.org/0000-0002-4218-1191, Moore, L., Connerney, J. E. P., Melin, H., Stallard, T. S., Miller, S. and Baines, K. H. (2017) Redetection of the ionospheric signature of Saturn's "Ring Rain". Geophysical Research Letters, 44 (23). 11,762-11,769. ISSN 1944-8007 doi: 10.1002/2017GL075932 Available at https://centaur.reading.ac.uk/120088/

AGU PUBLICATIONS

Geophysical Research Letters

RESEARCH LETTER
10.1002/2017GL075932

Key Points:
- H_3^+ emissions from Saturn's ionosphere were analyzed using recently acquired Keck telescope observations
- Anomalous nonsolar variations in H_3^+ emissions were detected, consistent with the transport of "rain" from Saturn's rings to the atmosphere
- H_3^+ intensities peak near 43, 51, and 63° planetocentric latitude north, some near proposed latitudes of increased water influx

Supporting Information:
- Supporting Information S1

Correspondence to:
J. O'Donoghue,
j.odonoghue@nasa.gov

Citation:
O'Donoghue, J., Moore, L., Connerney, J. E. P., Melin, H., Stallard, T. S., Miller, S., & Baines, K. H. (2017). Redetection of the ionospheric H_3^+ signature of Saturn's "ring rain". *Geophysical Research Letters*, *44*, 11,762–11,769. https://doi.org/10.1002/2017GL075932

Received 4 OCT 2017
Accepted 15 NOV 2017
Accepted article online 20 NOV 2017
Published online 11 DEC 2017

Redetection of the Ionospheric H_3^+ Signature of Saturn's "Ring Rain"

James O'Donoghue[1], Luke Moore[2], John E. P. Connerney[1], Henrik Melin[3], Tom S. Stallard[3], Steve Miller[4], and Kevin H. Baines[5]

[1]Planetary Magnetospheres Laboratory, NASA Goddard Space Flight Center, Greenbelt, MD, USA, [2]Center for Space Physics, Boston University, Boston, MA, USA, [3]Department of Physics and Astronomy, University of Leicester, Leicester, UK, [4]Atmospheric Physics Laboratory, Department of Physics and Astronomy, University College London, London, UK, [5]NASA Jet Propulsion Laboratory, Pasadena, CA, USA

Abstract In April 2011 Saturn's midlatitude ionospheric H_3^+ emissions were detected, exhibiting anomalous (nonsolar) H_3^+ latitudinal variations consistent with the transport of water from specific locations in Saturn's rings, known as "ring rain". These products, transported to the planet along the magnetic field, may help to explain the unusual pattern of peaks and troughs in electron densities discovered in Saturn's ionosphere by spacecraft flybys. In the present study, we analyzed H_3^+ emissions recorded on 23 April 2013, showing for the first time since the original detection that Saturn's midlatitude H_3^+ emissions are indeed heavily modified. Although the 2013 emissions are dimmer by almost a factor of 3.7, the latitudinal contrast is greater and uncertainties are lower. Increased H_3^+ intensities were found near planetocentric latitudes of 43°, 51°, and 63°, previously identified with sources at the inner edge of the B ring, A ring, and the orbit of Enceladus and associated E ring.

Plain Language Summary Saturn was found in the past to be subjected to the flow of water particles from the rings to the planet, which leave an imprint on the upper parts of the atmosphere. This water is eroded from Saturn's rings by a combination of electrical and magnetic forces, which can alter the estimated age and lifetime of the rings. Here we present our observations that have redetected this influence upon the atmosphere at higher resolution, significantly improving our understanding of how it works.

1. Introduction

Prior to the arrival of any spacecraft at Saturn, early models describing Saturn's ionosphere based on photoionization of H_2, He, and H by extreme ultraviolet (EUV) radiation from the Sun predicted an electron density of around 1×10^5 cm^{-3} (McElroy, 1973; Waite et al., 1979). In 1979, the Pioneer 11 spacecraft became the first human-made object to encounter Saturn as it flew by (Kliore et al., 1980). The spacecraft was occulted twice by Saturn: once upon passing behind the planet at 11.6° south latitude, and again as it emerged 1 h 19 min later at 9.6° south. Kliore et al. (1980) used the radio occultations to estimate the ionospheric electron density as a function of altitude, finding that the peak density was an order of magnitude less than models predicted, at 1×10^4 cm^{-3}.

Subsequent radio occultations by Voyager 1 and 2, in 1980 and 1981, showed peak electron densities between $\sim6\times10^3$ cm^{-3} and $\sim2.3\times10^4$ cm^{-3} (Atreya et al., 1984). The highest density was derived at a latitude of 73° south, while the lowest was found at 36° north, an unexpected latitudinal variation. Nonauroral peak electron densities ought to increase toward the equator as their production mechanism is solar EUV ionization. Likewise, analyses of Saturn electrostatic discharges suggested dramatic variations of peak electron density with both latitude and local time Kaiser et al. (1984).

Connerney and Waite (1984) proposed a "radically different" ionospheric model to account for these observations in which an exogenous water influx was introduced, greatly accelerating recombination and depleting peak densities. They found that a planet-wide water influx of $\sim4\times10^7$ molecules cm^{-2} s^{-1} was needed in order to reduce electron densities to match the observed values. A much greater localized water influx magnetically conjugate to the inner edge of the B ring (−38° south) was also proposed. This source was required to explain

observed latitudinal variations in peak density but was also predicted by a theory of charged particle motion in Saturn's ring plane (Northrop & Hill, 1983).

An influx of water transported along the magnetic field from the rings would result in latitudinal variations in ionospheric chemistry and electron density (Connerney & Waite, 1984). Saturn's ring system contains submicrometer-sized ice particles or icy grains that can acquire charge by photoionization or exposure to a micrometeorite impact's dense plasma cloud (Connerney, 2013). On acquiring charge, sufficiently high charge-to-mass ratio grains are confined to motion along the magnetic field, in response to gravitational, centrifugal, and magnetic mirror forces acting on the grain (Connerney, 2013; Northrop & Connerney, 1987; Northrop & Hill, 1983). Inward of 1.62 R_S (where 1 R_S is Saturn's equatorial radius 60,268 km) within the ring plane, charged grains with zero magnetic moment are unstable and will not return to the rings and be reabsorbed. At radial distances less than 1.62 R_S, gravity overwhelms centrifugal force (resolved along B), pulling charged grains along B toward the planet (Northrop & Hill, 1983). Charged grains initially moving at Keplerian velocity will experience a magnetic mirror force in addition to gravity and centrifugal forces, which acts to reflect charged grains back to the rings, such that the original 1.62 R_S force balance region is moved closer to the planet at 1.525 R_S in the ring plane (Connerney, 2013; Northrop & Connerney, 1987; Northrop & Hill, 1983).

This process is perhaps best described as an electromagnetic erosion process that over time depletes the rings. Indeed, the boundary between the B and C rings at 1.525 R_S exhibits a sharp transition in density; "ring rain" may very well explain the bulk structure of the rings (Northrop & Connerney, 1987). A similar process involving positively charged dust grains has been modeled, demonstrating a pathway for an influx of water into the equatorial ionosphere (Liu & Ip, 2014): this would help to explain the observed depletion in ionospheric electron density observed at the equator (Kliore et al., 2014). Estimating the mass loss of the rings by erosion mechanisms is of paramount importance for determining the age, lifetime, and evolution of the rings. Are they relatively young, with evolutionary lifetimes measured in tens of million years, or are they cosmogonic, a relic of solar system formation some 4.5 billion years ago (see Connerney, 2013, and references therein)?

Latitudinal variations in reflected light (high contrast, green filter Voyager 2 images) from Saturn's atmosphere were related to ring plane conjugate sources (Connerney, 1986a), suggesting transport along magnetic field lines. Dark bands in these images at 44.2° and 46.3° planetocentric latitude north map along magnetically field lines to suspected sources at 1.525 R_S and 1.62 R_S in the ring plane. Additional dark bands at 51.9° and 63.7° appear and are magnetically conjugate to, or near, the collection of gaps in the rings known as the Cassini division (starting at ~1.95 R_S) and to the orbit of Enceladus (3.95 R_S). Enceladus is a copious source of water in Saturn's magnetosphere, releasing water vapor at a rate of ~200 kg s^{-1} (Hansen et al., 2011). The reduction in reflected light associated with a local depletion of haze particles would result in dark bands; indeed, Connerney (1986a) proposed such a mechanism. Haze particles, acting as condensation nuclei for downward diffusing water, grow heavy enough to be depleted relative to neighboring latitudes.

Water was also directly observed in Saturn's atmosphere by the Infrared Space Observatory in the following decade, with Feuchtgruber et al. (1997) concluding that interplanetary dust (mostly originating from comets) and ring/satellite material are the likely sources. Hubble Space Telescope observations later showed that Saturn's hydrocarbon abundance exhibits a local minimum at 41° south, within a global trend of increasing toward the poles (Prangé et al., 2006). These results were reported to be consistent with a localized influx of water flowing into Saturn's atmosphere at latitudes magnetically linked to the rings, as photochemical models show that the presence of stratospheric water depletes hydrocarbon molecules (Moses & Bass, 2000).

H_3^+ is a major ion making up the ionosphere, with an observed peak density located at an altitude of ~1,155 km above the 1 bar pressure surface within the auroral region (Stallard et al., 2012). At lower latitudes, where auroral charged particle precipitation is not a factor, the modeled H_3^+ peak density may occur upward of 2,000 km above the 1 bar surface (Tao et al., 2011). The 10 m Keck II telescope on Mauna Kea, Hawaii, was used to observe emissions from H_3^+ ions from pole to pole in 2011 (O'Donoghue et al., 2013). Two broad and prominent peaks in H_3^+ intensity were found at planetocentric latitudes 43°N and 38°S, and as a result of the location of Saturn's magnetic equator lying north of the center of the planet by 0.036 R_S, both are conjugate to the same location in the ring plane near ~1.525 R_S (Connerney, 1986a). This was the first time that the predicted signature of ring rain was measured in both hemispheres simultaneously such that magnetic conjugacy was directly observed. This is particularly important as it demonstrates that the ionospheric emissions are related to magnetic conjugacy in the ring plane. The model of Moore et al. (2015) related the increase in H_3^+ emissions to an increase in H_3^+ density, as opposed to a temperature increase. They demonstrate that recombination of water

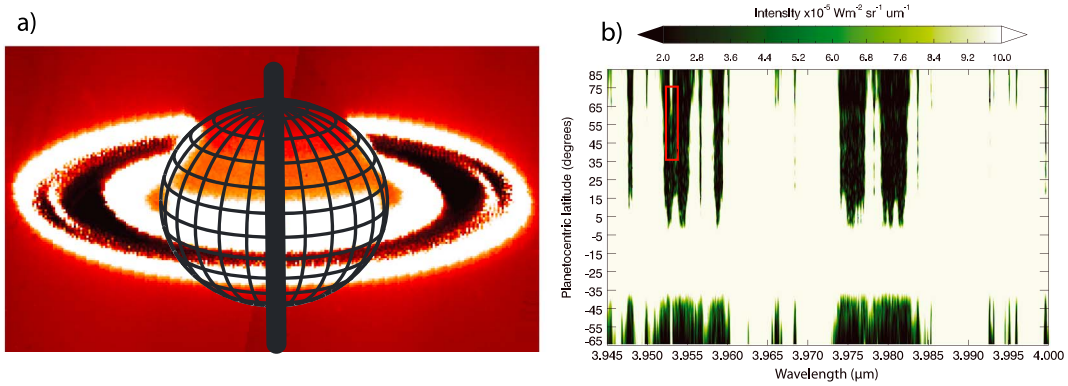

Figure 1. (a) Saturn as observed with Keck, 23 April 2013, using the NIRSPEC instrument's slit camera from a 2.134 to 2.5 μm^{-1} wavelength range. The slit of the spectrometer shown by the vertical black line in the middle of Figure 1a was orientated in the north-south position on Saturn, aligned along the rotational axis (Saturn's sub-Earth latitude was 18.3° during the observations). Light entering the slit is dispersed into spectral images. (b) The summation of all spectral images. Bright emissions at −15° planetocentric latitude (south) dominate the entire wavelength range and are the uniform reflection of sunlight by the rings, while the remaining bright areas are mostly due to reflection of sunlight by hydrocarbons. The vertical stripes of light at 3.953 μm^{-1} are the Q(1, 0$^-$) line emissions from H_3^+. The emissions from the red box are the focus of this study; this is the region depicted in Figure 2.

products (e.g., H_2O^+ and O^+) with electrons reduces the H_3^+ loss rate by the same process, yielding greater H_3^+ density in association with increased water influx.

Cassini spacecraft measurements of electron densities have not, thus far, tested the ring rain hypothesis, limiting the confidence needed to invest time in future study of the interaction (Kliore et al., 2014). Since the original detection of the H_3^+ modulation by ring rain, there have been no additional published observations of the phenomenon. This is due to two related factors: (1) Saturn's midlatitude thermosphere (colocated with the ionosphere) appears to have cooled by ~100 K between 2011 and 2015 (Koskinen et al., 2015); and (2) H_3^+ intensity is exponentially dependent upon the ion's temperature (Melin et al., 2014). These factors lead to a

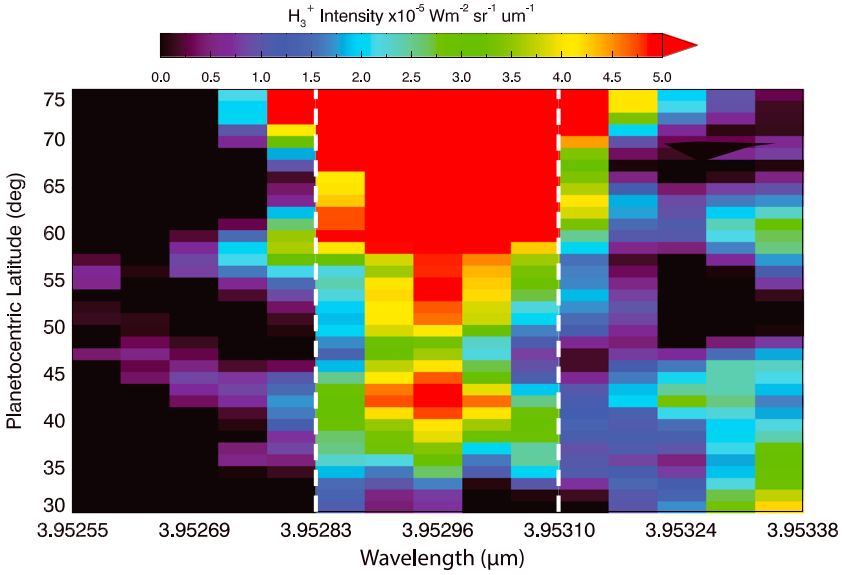

Figure 2. A spectral image of Saturn's intensity from 2013 observations as a function of northern planetocentric latitude (*y* axis) and wavelength (*x* axis). Color contours indicate the intensity of light received at the detector, with emissions higher than 5×10^{-5} Wm^{-2} sr^{-1} μm^{-1} limited to this value. Centered at 3.95296 μm is the fundamental H_3^+ emission line, Q(1, 0$^-$). Vertical dashed lines (white) indicate the area selected for investigating H_3^+ intensity as a function of latitude. Emissions outside of the area indicated by the dashed lines are primarily hydrocarbon reflection of sunlight and secondarily the background noise.

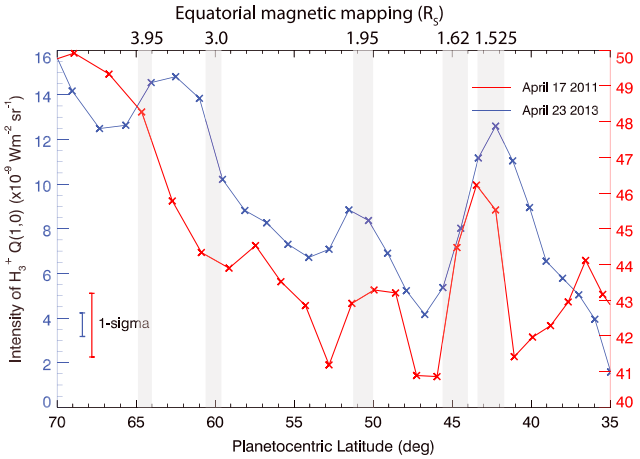

Figure 3. Saturn's H_3^+ Q(1, 0$^-$) line intensities (*y* axis) as a function of north planetocentric latitude (*x* axis). The 2013 line intensity results from the summation of light between the vertical dashed lines in Figure 2. The 2011 line intensities are summed from the same wavelengths, corresponding to a FWHM of 5 pixels in each data set, enough to encompass the majority of the line emission without gathering appreciable noise from other wavelengths. The top horizontal axis and vertical red lines indicate the corresponding ring plane conjugate distances. From left to right, these correspond to the inner edge of the E ring and orbit of Enceladus (3.0 R_S–3.95 R_S), the Cassini division (starting at ~1.95 R_S), and the two theoretical water source locations (1.62 R_S and 1.525 R_S) discussed in the main text. Note the range of possible conjugates taking into account different magnetic field models, altitude of emission, and observation uncertainties. One-sigma uncertainties are calculated based on the background intensity in the spectral image (where no hydrocarbon reflection is present).

decrease in signal strength of H_3^+ at midlatitudes over time, with more recent observations obtained near the limit of detection. However, owing to improved data reduction and analysis, applied to ground-based Keck telescope data from 2013, we present the first redetections of the apparent imprint of ring rain on Saturn's ionospheric H_3^+.

2. Observations

We present observations of Saturn's midlatitude H_3^+ emissions obtained with the 10 m Keck telescope on 23 April 2013, between 10:30 and 13:40 Universal Time (UT). We also performed a reanalysis of data from the 17 April 2011 observing opportunity (O'Donoghue et al., 2013), to ensure that a comparison between the two used an identical data reduction approach. However, almost all of the results and discussion herein are related to the 2013 campaign (Melin et al., 2016) (refer to O'Donoghue et al. (2013) for details on the 2011 observations). One of the largest differences between these two observing opportunities is the planetary tilt with respect to the Earth, which was 8.2° in 2011 and 18.3° in 2013. The 2011 observations afforded the ability to view both hemispheres simultaneously; those in 2013 are limited to northern latitudes only, as the southern hemisphere is largely obscured by the rings. The 2013 observations do show a modest improvement in spatial resolution in the north: at 67.7° a single pixel subtends 2° of latitude in 2011, whereas in 2013, the same pixel represents 1.5°. The influence of planetary tilt on spatial resolving power becomes negligible when heading equatorward to 35°, with the difference in resolution per pixel is less than 0.1°.

The Near InfraRed SPECtrometer (NIRSPEC, McLean et al., 1998) was used on Keck II. The detector's 24 by 0.432 arc second spectrometer slit (1 pixel corresponds to 0.144 arc seconds in the resulting images) was orientated along Saturn's noon meridian in a north-south direction as shown in Figure 1a. NIRSPEC has a resolving power of R = $\lambda/\Delta\lambda$ ~25,000, providing a minimum spectral resolution of, for example, $\Delta\lambda \approx 1.59\times10^{-4}$ μm at 3.975 μm. Exposures were taken as the planet rotated beneath the slit, such that during the night of observation light from 39 to 135° Central Meridian Longitude (in the Saturn system III longitude system, Kaiser et al., 1980) was captured. The result of coadding the 50 frames recorded on 23 April 2013 is shown in Figure 1b. Atmospheric seeing was estimated to be 0.4 and 0.7″ in 2011 and 2013, respectively. Other observations in the April 2013 campaign took place on 19–21 April but were directed toward Saturn's auroral/polar regions (O'Donoghue et al., 2015).

The telescope slewed to two positions throughout the night: Saturn "A" and sky "B," in an ABBA pattern. At each position a spectral image was obtained, consisting of twelve 5 s integrations, yielding 60 s exposures. Standard astronomical reduction techniques were used to clean the spectral images; we outline the main ones here. The most important process (causing the largest improvement) is A-minus-B subtraction in which the Earth's sky emissions are removed from the Saturn spectra. A flux calibration was performed by measuring the spectrum of a standard (blackbody emitting) star (A0) to obtain the physical flux per photodetector count rate. This has a dual benefit in that it also accounts for the wavelength-dependent absorption of light by the Earth's atmosphere. The stars used for performing the calibrations in the 2011 and 2013 were HR6035 and HR7891, respectively. A dark current subtraction and a division by a "flat field" frame were performed to account for thermal emissions at the detector and nonuniformity in the response of the detector and optics, respectively.

3. Analysis and Results

A total of 50 cleaned and flux-calibrated Saturn frames were aligned and coadded to make a single spectrum for the analysis of 2013 data, and 38 frames in the 2011 reanalysis. A Gaussian curve was first fitted to the large and bright rings (which emit at all measured wavelengths) in the spectral image to assign pixels to latitudes. The decrease in intensity of planetary emissions was mapped poleward from that position until

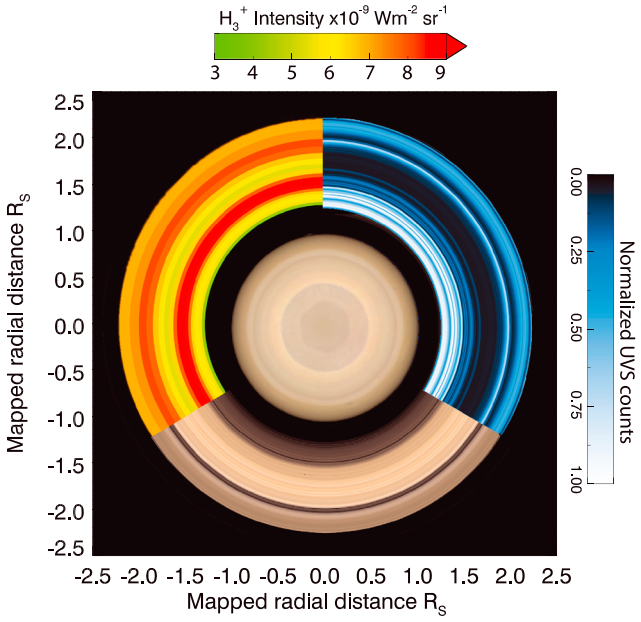

Figure 4. Saturn and its planetary ring system is shown from above the northern pole. Both axes show the radial distances from the center of the planet. H_3^+ intensities from Figure 3 (capped to 9 nWm^{-2} sr^{-1}) are traced via the magnetic field to their mapped radial distances in the ring plane on the upper left of the rings (over an arbitrary range of longitudes). On the top right, ring opacity measured by the Voyager 2 UVS is shown (Lane et al., 1982; Lillie et al., 1977). At the bottom, for context, a portion of Saturn's rings observed in reflected light is shown.

reaching near zero at the planetary limbs north and south. The limb-to-limb distance in pixels (118 pixels) equates to 17 arc seconds, and together with the geometry obtained from planetary ephemeris (NASA's Horizons web interface at https://ssd.jpl.nasa.gov/horizons.cgi), planetocentric latitudes were assigned. Telluric seeing adds uncertainty in determining the position of the planetary limb, since the data are spatially smeared by ±2 pixels (±0.3″). This uncertainty equates to ∼1° of latitude near 35° north, increasing to 3° by 75° north due to the variation in viewing geometry. A cosine correction of the emission angle was applied to remove the line-of-sight effects of viewing geometry.

In order to map planetary latitudes to radial distance in the ring plane, magnetic field lines are traced from the ionosphere to the ring plane using a model of Saturn's magnetosphere. We used two different sets of spherical harmonic coefficients, one set based on Voyager 2 spacecraft derived data and the other on Cassini spacecraft data. Both models are the same except for the difference in coefficients and include the full order-3 internal field, ring current, oblateness of the planet, and a Saturn equatorial radius of 1 R_s = 60,268 km. A range of ionospheric heights of 1,155–2,155 km were used to account for the unknown level of the H_3^+ density peak from low-to-high-latitudes (Stallard et al., 2012; Tao et al., 2011). The Voyager "Z3" magnetic mapping model of Connerney et al. (1982) was used with the coefficients g1 = 21,248 nT, g2 = 1,613, and g3 = 2683 (evaluated at 1 R_S), while the Cassini model used internal field coefficients g1 = 21,153 nT, g2 = 1,576, and g3 = 2,267 from Burton et al. (2010). The Z3 model maps a given equatorial radial distance in the rings slightly poleward (∼ 1°) of estimates obtained using the Cassini model, while the range of ionospheric height estimates broadens mapping solutions toward the equator. The range of mappings from both models for the full range of altitudes is illustrated by the grey bars in Figure 3.

A portion of the coadded spectral image is shown in Figure 2, in which the fundamental H_3^+ Q(1, 0$^-$) line emission at 3.9529 μm can be seen as a function of wavelength and latitude. The strongest emissions are associated with greater density and/or temperature of ionospheric-bound H_3^+. The highest latitudes are the most intense: these are the auroral regions centered at ∼ 75° (Badman et al., 2006). Equatorward of the aurorae (and the focus of this study), the decrease in intensity toward the equator is interrupted by bright features near ∼ 51° and ∼ 44°. The full width at half maximum (FWHM) power of the nonauroral Q(1, 0$^-$) spectral line is shown by white dashed lines; the area inside is summed and plotted against latitude in Figure 3. From 2011 to 2013, the maximum intensity of H_3^+ between 42° and 45° has decreased by a factor of 3.7.

The two northern planetocentric latitudes upon which ring-derived water is theoretically expected to fall are at 45° and 42° and correspond to 1.62 R_S and 1.525 R_S, respectively, when mapped to the equatorial plane. In both Figures 2 and 3 we observe a large increase in Q(1, 0$^-$) intensity centered within these locations. Additionally, two prominent nonauroral peaks in intensity are visible: one at 51° and one near 63°. The former maps close to the Cassini division, whereas the latter maps to a region occupied by Enceladus and the inner edge of the E ring. These H_3^+ emission intensity enhancements correspond to the four features (dark bands) identified in Saturn's northern hemisphere (Connerney, 1986a) and attributed to an increased water influx. Vertical grey regions in Figure 3 mark these mappings of significant interest, noting that the latitudinal ranges of these regions are due to uncertainties in the position of the mapping (see section 3).

In order to demonstrate the relationship between ionospheric H_3^+ and ring structures, in Figure 4 we take the planetary emissions from Figure 3 and trace them via the magnetic field and cast them onto Saturn's rings. This is shown alongside an illustration of ring opacity from a stellar occultation of the rings by the Voyager 2 Ultraviolet Spectrometer (UVS) (Lane et al., 1982; Lillie et al., 1977). A value of 0 indicates that the rings were sufficiently dense to block all UV photons from the star "behind" the rings, while a value of 1 indicates light is passing through unhindered.

4. Interpretation and Discussion

Saturn's midlatitude H_3^+ emissions appear to be inextricably associated with features in the ring plane. The results presented here are the first confirmation of the modulation of ionospheric H_3^+ by virtue of an interaction with Saturn's rings (ring rain), as originally found by O'Donoghue et al. (2013) using data from 2011. A major difference between these two sets of observations, separated by 2 years, is the planetwide decrease in intensity of the ionospheric emissions. Near 42° they are a factor of ~3.7 weaker in the more recent observations. This fact explains the lack of success, until now, in redetecting any H_3^+ signal in that region in 2013. It is likely due to a decrease in the upper-atmospheric temperature (~100 K) from 2011 to 2013, as observed by Koskinen et al. (2015) during this period. Based on measurements by Koskinen et al. (2015), we estimate that the exospheric temperature near northern midlatitudes in our H_3^+ measurements was 500 K. Assuming that the H_3^+ temperature is 20 K lower than this (Moore et al., 2015), we estimate that a factor of 3.7 difference in the signal strength represents a 90 K drop in temperature. We calculate that the H_3^+ temperature in 2013 ought to be near 390 K (assuming there are no changes in density; see the supporting information for further details). However, because density and temperature may both vary at the same time, only direct measurements of H_3^+ temperatures and densities can confirm this. This measurement is only possible if one can observe 2 or more H_3^+ lines; only the Q(1,0) line emission was visible in 2013. Most of the emission peaks and troughs found in H_3^+ Q(1, 0^-) intensity in 2013 appear to occur at comparable latitudes as observed in 2011, within observational uncertainties. The results from 2013 show a more highly resolved latitudinal variation compared with 2011, as shown by Figure 3, with a larger contrast between bright and dim features and lower uncertainties. This may reflect the better spatial resolution realized in the more recent observations or differences in observing conditions that could not be accurately measured throughout the night. Entertaining a physical basis for the differences would be rather premature, though it would presumably involve increased precipitation of water in 2013 compared to 2011.

An influx from the rings (1.525 R_S and 1.62 R_S) is the most likely reason for the relatively higher H_3^+ emissions near 42°N latitude (Northrop & Connerney, 1987; O'Donoghue et al., 2013). H_3^+ intensity enhancements were modeled assuming increased number of H_3^+ ions emitting, as opposed to higher ion temperatures that yield a larger emission per ion (Moore et al., 2015). This is because the introduction of water products reduces electron densities locally, thus, reducing the major loss mechanism of H_3^+ (recombination with electrons). Overall, this causes H_3^+ densities and therefore emissions to be greatest when colocated with an enhanced water influx. H_3^+ density is treated as the main driver of emissions based on the available data, since a flow of water from 1.525 R_S is expected (Northrop & Connerney, 1987; Northrop & Hill, 1982), observed (Connerney, 1986a; O'Donoghue et al., 2013), and modeled to increase the density of H_3^+ (Moore et al., 2015). In the supporting information we explore the H_3^+ emissions further, varying density at fixed temperature, and varying temperature at fixed density. The H_3^+ temperatures and densities in 2013 are considerably more variable than those of 2011, but that it is difficult to draw further conclusions due to the covariability of temperature and density in emission intensity.

Two discrete dark bands were identified in images from Voyager 2 (Connerney, 1986a), associated with the inner B ring, while here we observe only one peak of H_3^+ Q(1, 0^-) located near 43°. The peak of intensity near 43° leans slightly equatorward of the predicted conjugate of the inner edge of the B ring (but within observational uncertainties of 1–2°). The flux of water-bearing grains available for transport from the rings depends on (1) whether charged grains can be trapped in the ring plane (and reabsorbed before transport) and (2) the number of small grains available to be charged. Inside of 1.525 R_S, charged grains must fall into the planet, but as the C ring is less dense than the B ring, and largely devoid of small particles—likely as a consequence of the ring rain erosion mechanism itself—it makes for a poor source region. Outward of 1.525 R_S, charged grains can be trapped and reabsorbed before loss, but there is a copious supply of small grains available in the optically dense B ring. At 1.525 R_S, there is a "best of both worlds" scenario: a rich supply of grains available to be charged and a low trapping potential. This presumes that the optically thick B ring is able to transport particles inward to replace those lost. Our data are smoothed by the latitudinal seeing of ±2°, so we may simply lack the resolution required to identify discrete sources in close proximity. This limitation may be overcome using adaptive optics or by observing from space, with, for example, the James Webb Space Telescope.

5. Summary

We analyzed H_3^+ emissions from Saturn's northern hemisphere taken by the Keck telescope in 23 April 2013. We found that Saturn's midlatitude ionosphere is dominated by interactions with the ring system via the magnetic field, replicating the observational results of O'Donoghue et al. (2013) for the first time and partially explaining the unusual electron densities found at Saturn (Kliore et al., 2014). All of the H_3^+ intensity enhancements seen here are colocated with dark bands observed in images from the Voyager 2 spacecraft, attributed to the removal of stratospheric haze by an influx of water from the rings (Connerney, 1986a). The theoretical water sources in the rings at 1.525 R_S and 1.62 R_S are associated with a single latitudinally broad peak in H_3^+ intensity near 43° planetocentric latitude north. The peak in H_3^+ intensity itself likely indicates that downward diffusing water increases H_3^+ density through a chain of chemical reactions and electron recombination (Moore et al., 2015). The midlatitude emissions near 63° reported by Stallard et al. (2008, 2010) were also observed, suggestive of water influx from Enceladus and the associated E ring (Connerney, 1986a). Data garnered from the final orbits of the Cassini spacecraft will likely add much information about the nature of the ring-magnetosphere-ionosphere coupling at Saturn (Connerney, 1986b). With no spacecraft in orbit around Saturn, and none in the planning stages, it may be up to ground-based observations to provide insight into the electromagnetic ring-erosion mechanism, which has a bearing on the age, lifetime, and evolution of the rings.

Acknowledgments

James O'Donoghue's research was supported by an appointment to the National Aeronautics and Space Administration (NASA) Postdoctoral Program at the NASA Goddard Space Flight Center, administered by Universities Space Research Association under contract with NASA. This material is based upon work supported by NASA under grants NNX14AG72G and NNX17AF14G issued through the SSO Planetary Astronomy Program. Henrik Melin and Tom Stallard were supported by the Science and Technology Facilities Council under grant ST/K001000/1. The data presented herein were obtained at the W. M. Keck Observatory, which is operated as a scientific partnership among the California Institute of Technology, the University of California, and NASA, and the data in the form of fits files are available from the Keck archive at https://www2.keck.hawaii.edu/koa/public/koa.php. We are grateful to the staff at the Keck Observatory. The authors wish to recognize the significant cultural role and reverence that the summit of Mauna Kea has within the indigenous Hawaiian community: we are fortunate to have the opportunity to conduct observations from this mountain.

References

Atreya, S. K., Donahue, T. M., Nagy, A. F., Waite Jr., J. H., & McConnell, J. C. (1984). Theory, measurements, and models of the upper atmosphere and ionosphere of Saturn. In T. Gehrels (Ed.), *Saturn* pp. 239–277). Tucson, AZ: University of Arizona Press.

Badman, S. V., Cowley, S. W. H., Gérard, J.-C., & Grodent, D. (2006). A statistical analysis of the location and width of Saturn's southern auroras. *Annales Geophysicae*, *24*, 3533–3545. https://doi.org/10.5194/ angeo-24-3533-2006

Burton, M. E., Dougherty, M. K., & Russell, C. T. (2010). Saturn's internal planetary magnetic field. *Journal of Geophysical Research*, *37*, L24105. https://doi.org/10.1029/2010GL045148

Connerney, J. (2013). Solar system: Saturn's ring rain. *Nature*, *496*, 178–179. https://doi.org/10.1038/496178a

Connerney, J. E. P. (1986a). Magnetic connection for Saturn's rings and atmosphere. *Geophysical Research Letters*, *13*, 773–776. https://doi.org/10.1029/GL013i008p00773

Connerney, J. E. P. (1986b). Saturn—A unique magnetosphere/ionosphere/ring interaction, *Comparative study of magnetospheric systems; International Colloquium, Londe-les-Maures, France* pp. 245–251). Toulouse, France: Cepadues-Editions.

Connerney, J. E. P., & Waite, J. H. (1984). New model of Saturn's ionosphere with an influx of water from the rings. *Nature*, *312*, 136–138. https://doi.org/10.1038/312136a0

Connerney, J. E. P., Ness, N. F., & Acuna, M. H. (1982). Zonal harmonic model of Saturn's magnetic field from Voyager 1 and 2 observations. *Nature*, *298*, 44–46. https://doi.org/10.1038/298044a0

Feuchtgruber, H., Lellouch, E., de Graauw, T., Bézard, B., Encrenaz, T., & Griffin, M. (1997). External supply of oxygen to the atmospheres of the giant planets. *Nature*, *389*, 159–162. https://doi.org/10.1038/38236

Hansen, C. J., Shemansky, D. E., Esposito, L. W., Stewart, A. I. F., Lewis, B. R., Colwell, J. E., … Magee, B. A. (2011). The composition and structure of the Enceladus plume. *Geophysical Research Letters*, *38*, L11202. https://doi.org/10.1029/2011GL047415

Kaiser, M. L., Desch, M. D., Warwick, J. W., & Pearce, J. B. (1980). Voyager detection of nonthermal radio emission from Saturn. *Science*, *209*, 1238–1240. https://doi.org/10.1126/science.209.4462.1238

Kaiser, M. L., Desch, M. D., & Connerney, J. E. P. (1984). Saturn's ionosphere—Inferred electron densities. *Journal of Geophysical Research*, *89*, 2371–2376. https://doi.org/10.1029/JA089iA04p02371

Kliore, A. J., Patel, I. R., Lindal, G. F., Sweetnam, D. N., Hotz, H. B., Waite, J. H., & McDonough, T. (1980). Structure of the ionosphere and atmosphere of Saturn from Pioneer 11 Saturn radio occultation. *Journal of Geophysical Research*, *85*, 5857–5870. https://doi.org/10.1029/JA085iA11p05857

Kliore, A. J., Nagy, A., Asmar, S., Anabtawi, A., Barbinis, E., Fleischman, D., … Klose, J. (2014). The ionosphere of Saturn as observed by the Cassini Radio Science System. *Geophysical Research Letters*, *41*, 5778–5782. https://doi.org/10.1002/2014GL060512

Koskinen, T. T., Sandel, B. R., Yelle, R. V., Strobel, D. F., Müller-Wodarg, I. C. F., & Erwin, J. T. (2015). Saturn's variable thermosphere from Cassini/UVIS occultations. *Icarus*, *260*, 174–189. https://doi.org/10.1016/j.icarus.2015.07.008

Lane, A. L., Hord, C. W., West, R. A., Esposito, L. W., Coffeen, D. L., Sato, M., … Morris, R. B. (1982). Photopolarimetry from Voyager 2—Preliminary results on Saturn, Titan, and the rings. *Science*, *215*, 537–543. https://doi.org/10.1126/science.215.4532.537

Lillie, C. F., Hord, C. W., Pang, K., Coffeen, D. L., & Hansen, J. E. (1977). The Voyager mission photopolarimeter experiment. *Space Science Reviews*, *21*, 159–181. https://doi.org/10.1007/BF00200849

Liu, C.-M., & Ip, W.-H. (2014). A new pathway of Saturnian ring-ionosphere coupling via charged nanograins. *Astrophysical Journal*, *786*, 34. https://doi.org/10.1088/0004-637X/786/1/34

McElroy, M. B. (1973). The ionospheres of the major planets (Article published in the Space Science Reviews special issue on 'Outer Solar System Exploration—An Overview', ed. by J. E. Long and D. G. Rea). *Space Science Reviews*, *14*, 460–473. https://doi.org/10.1007/BF00214756

McLean, I. S., Becklin, E. E., Bendiksen, O., Brims, G., Canfield, J., Figer, D. F., … Wong, W. (1998). Design and development of NIRSPEC: A near-infrared echelle spectrograph for the Keck II telescope. In A. M. Fowler (Ed.), *Proceedings of the Society of Photo-Optical Instrumentation Engineers (SPIE) conference series* (Vol. 3354, pp. 566–578), Kona, HI: Astronomical Telescopes and Instrumentation, Infrared Astronomical Instrumentation.

Melin, H., Stallard, T. S., O'Donoghue, J., Badman, S. V., Miller, S., & Blake, J. S. D. (2014). On the anticorrelation between H_3^+ temperature and density in giant planet ionospheres. *Monthly Notices of the Royal Astronomical Society*, *438*, 1611–1617. https://doi.org/10.1093/mnras/stt2299

Melin, H., Badman, S., & Khurana, K. (2016). The 2013 Saturn auroral campaign. *Icarus*, *263*, 1–1. https://doi.org/10.1016/j.icarus.2015.09.028

Moore, L., O'Donoghue, J., Müller-Wodarg, I., Galand, M., & Mendillo, M. (2015). Saturn ring rain: Model estimates of water influx into Saturn's atmosphere. *Icarus*, *245*, 355–366. https://doi.org/10.1016/j.icarus.2014.08.041

Moses, J. I., & Bass, S. F. (2000). The effects of external material on the chemistry and structure of Saturn's ionosphere. *Journal of Geophysical Research*, *105*, 7013–7052. https://doi.org/10.1029/1999JE001172

Northrop, T. G., & Connerney, J. E. P. (1987). A micrometeorite erosion model and the age of Saturn's rings. *Icarus*, *70*, 124–137. https://doi.org/10.1016/0019-1035(87)90079-0

Northrop, T. G., & Hill, J. R. (1982). Stability of negatively charged dust grains in Saturn's ring plane. *Journal of Geophysical Research*, *87*, 6045–6051. https://doi.org/10.1029/JA087iA08p06045

Northrop, T. G., & Hill, J. R. (1983). The inner edge of Saturn's B ring. *Journal of Geophysical Research*, *88*, 6102–6108. https://doi.org/10.1029/JA088iA08p06102

O'Donoghue, J., Stallard, T. S., Melin, H., Jones, G. H., Cowley, S. W. H., Miller, S., … Blake, J. S. D. (2013). The domination of Saturn's low-latitude ionosphere by ring 'rain'. *Nature*, *496*, 193–195. https://doi.org/10.1038/nature12049

O'Donoghue, J., Melin, H., Stallard, T. S., Provan, G., Moore, L., Badman, S. V., … Blake, J. S. D. (2015). Ground-based observations of Saturn's auroral ionosphere over three days: Trends in H_3^+ temperature, density and emission with Saturn local time and planetary period oscillation. *Icarus*, *263*, 44–55. https://doi.org/10.1016/j.icarus.2015.04.018

Prangé, R., Fouchet, T., Courtin, R., Connerney, J. E. P., & McConnell, J. C. (2006). Latitudinal variation of Saturn photochemistry deduced from spatially-resolved ultraviolet spectra. *Icarus*, *180*, 379–392. https://doi.org/10.1016/j.icarus.2005.11.005

Stallard, T., Miller, S., Melin, H., Lystrup, M., Cowley, S. W. H., Bunce, E. J., … Dougherty, M. (2008). Jovian-like aurorae on Saturn. *Nature*, *453*, 1083–1085. https://doi.org/10.1038/nature07077

Stallard, T., Melin, H., Cowley, S. W. H., Miller, S., & Lystrup, M. B. (2010). Location and magnetospheric mapping of Saturn's mid-latitude infrared auroral oval. *Astrophysical Journal*, *722*, L85—L89. https://doi.org/10.1088/2041-8205/722/1/L85

Stallard, T. S., Melin, H., Miller, S., O' Donoghue, J., Cowley, S. W. H., Badman, S., … Baines, K. H. (2012). Temperature changes and energy inputs in giant planet atmospheres: What we are learning from H_3^+. *Philosophical Transactions of the Royal Society of London, Series A: Mathematical, Physical and Engineering Sciences*, *370*, 5213–5224. https://doi.org/10.1098/rsta.2012.0028

Tao, C., Badman, S. V., & Fujimoto, M. (2011). UV and IR auroral emission model for the outer planets: Jupiter and Saturn comparison. *Icarus*, *213*, 581–592. https://doi.org/10.1016/j.icarus.2011.04.001

Waite, J. H., Atreya, S. K., & Nagy, A. F. (1979). The ionosphere of Saturn—Predictions for Pioneer 11. *Geophysical Research Letters*, *6*, 723–726. https://doi.org/10.1029/GL006i009p00723